

Optimal layout of a partially treated laminated composite magnetorheological fluid sandwich plate

R. Manoharan, R. Vasudevan* and A.K. Jeevanantham

School of Mechanical and Building Sciences, VIT University, Vellore - 632014, India

(Received March 24, 2015, Revised July 26, 2015, Accepted September 26, 2015)

Abstract. In this study, the optimal location of the MR fluid segments in a partially treated laminated composite sandwich plate has been identified to maximize the natural frequencies and the loss factors. The finite element formulation is used to derive the governing differential equations of motion for a partially treated laminated composite sandwich plate embedded with MR fluid and rubber material as the core layer and laminated composite plate as the face layers. An optimization problem is formulated and solved by combining finite element analysis (FEA) and genetic algorithm (GA) to obtain the optimal locations to yield maximum natural frequency and loss factor corresponding to first five modes of flexural vibration of the sandwich plate with various combinations of weighting factors under various boundary conditions. The proposed methodology is validated by comparing the natural frequencies evaluated at optimal locations of MR fluid pockets identified through GA coupled with FEA and the experimental measurements. The converged results suggest that the optimal location of MR fluid pockets is strongly influenced not only by the boundary conditions and modes of vibrations but also by the objectives of maximization of natural frequency and loss factors either individually or combined. The optimal layout could be useful to apply the MR fluid pockets at critical components of large structure to realize more efficient and compact vibration control mechanism with variable damping.

Keywords: composites; MR fluid; MR fluid Sandwich plate; FEA; vibration; optimization

1. Introduction

Multi layered composite sandwich plate has been used in aircraft and aerospace engineering applications for more than 40 years due to their high bending stiffness and strength to small weight ratios, long fatigue life, low maintenance cost and resistance to electrochemical corrosion. It is necessary to develop the reliable and practical models to predict the static and dynamic behavior of the structure. Semi-active control devices have been proposed for structural control applications (Carlson and Weiss 1994, See 2004) because it has more advantages compared to active and passive control devices. These devices include controllable fluids such as electro-rheological (ER) and magneto-rheological (MR) fluids which exhibit rapid change in their rheological properties and thus in the damping and stiffness properties with application of an electric or magnetic field. Generally the active control systems requires a significant amount of energy into the system while the semi-active control devices involve modifications of mechanical properties of the system in the

*Corresponding author, Professor, E-mail: vasudevan.r@vit.ac.in

preferred manner with only modest exterior energy (Dogruer *et al.* 2008). A lot of research works are being carried out to realize the effectiveness of semi-active damping control concepts for structural vibration control applications.

Many researchers have investigated experimentally and numerically the effectiveness of ER and MR fluid layers in controlling the vibration of the sandwich structures. Gandhi *et al.* (1989) developed the ER fluid based multi-functional, dynamically tunable semi active control devices to improve the structural damping ratio and the natural frequencies of the system. Leng *et al.* (1995) experimentally investigated the vibration analysis of ER fluid composite sandwich beam. It was concluded that the first three modes of natural frequencies and damping factors were increased with increasing the applied electric field. The vibration analysis of a fully and partially treated ER fluid sandwich beam was analyzed by Haiqing and King (1997) under clamped end conditions. The study concluded that the natural frequencies and loss factors of the sandwich beam depend on the length of ER fluid layer. Qiu and Khajika (1999) studied the vibration analysis of three-layered beams and five-layered beams with ER materials. It was concluded that the damping factor of a five-layer beam could be larger than that of a three-layer beam. Lee and Jwo (2001) experimentally analyzed the effect of spacing of parallel grooves on the local distribution of an electric field. Finite element methods were implemented to evaluate the structural stiffness and natural frequencies of the ER fluid sandwich plate with constrained layer (Yeh and Chen 2004). It was demonstrated that the stiffness of the sandwich plates could be controlled by varying the applied electric field and thickness of the ER layer. Yeh and Chen (2007) used the Hamilton's principle to investigate the vibration responses of an ER fluid based orthotropic sandwich plate. They concluded that the effect of natural frequencies and loss factor of the sandwich plate could be effectively controlled by the applied electric field, thickness of ER fluid layer and the constraining layer thickness. Yalcintas and Dai (1999, 2004) reported that MR fluid sandwich beam yields much higher natural frequencies with application of magnetic field than those of compared to ER under electric field. Sun *et al.* (2003) used the oscillatory rheometry techniques to develop the relationship between magnetic field and complex shear modulus of MR fluid. Also the dynamic responses of a MR fluid sandwich beam were analyzed by energy approach under various magnetic fields. The dynamic responses and dynamic instability of MR material based adaptive beam were studied by Yeh and Shih (2006) using DiTaranto sandwich beam theory and incremental harmonic balance method under axial harmonic load. Hu *et al.* (2006) developed the analytical model to predict the structural behavior of a MR fluid based sandwich beam under dynamic loading conditions. The natural frequencies and loss factors of the MR fluid sandwich beam were controlled by applied magnetic field strength and the vibration amplitudes are decreased by increasing applied magnetic field.

Lara-Prieto *et al.* (2010) investigated vibration responses of fully treated sandwich beam which was partially activated by permanent magnets. The vibration responses of a multi-layered MR fluid sandwich beam were investigated by Rajamohan *et al.* (2010a). Finite element method and Ritz formulations were used to derive the equations of motion of MR-fluid sandwich beam and validated through experimental test. Rajamohan *et al.* (2010b)] investigated a partially-treated MR fluid sandwich beam using finite element formulations and the natural frequencies were validated through the experimental investigation. Further the influence of locations of the MR fluid segments of a partially-treated MR fluid sandwich beam were investigated by Rajamohan *et al.* (2010c) using modal strain energy approach and finite element method under different end conditions. The optimal layouts of a partially treated MR fluid pocket in a sandwich beam were identified using genetic algorithm. It was shown that a relatively simple design could be realized

when the MR fluid is contained at a localized region. Rajamohan *et al.* (2011) investigated the optimal vibration control of fully and partially treated MR fluid sandwich beams using the linear quadratic regulator and flexible mode shape method. The dynamic responses of a rectangular plate with a magnetorheological fluid core and the isotropic constraining face layers were investigated using finite element method by Li *et al.* (2011). They concluded that the natural frequency increases while the loss factor decreases by increasing the applied magnetic field. The vibration characteristic of MR elastomer sandwich rectangular plates were analysed by Yeh (2013). It was concluded that the stiffness of the sandwich plate could be controlled by varying the applied magnetic field and the thickness of MR elastomer core layer.

Manoharan *et al.* (2014a) analyzed the dynamic characterization of a laminated composite MR fluid sandwich plate. The governing differential equations of motion of a sandwich plate were developed using finite element formulation and the natural frequency and loss factor were analyzed by varying the magnetic field intensities. Manoharan *et al.* (2014b) presented the finite element formulations for a partially-treated laminated composite MR fluid sandwich plate comprising various MR-fluid pockets under various boundary conditions. The study suggested that the location and size of the MR fluid pockets have significant effect on the natural frequencies and the loss factors apart from the intensity of the applied magnetic field and the boundary conditions. Even though few research works have been carried out to investigate the effectiveness of partial treatment MR fluid in an isotropic and laminated composite plates, the identification of optimal locations of a MR fluid pockets in a laminated composite sandwich plate is yet to be explored.

In the present study, the optimal locations of MR fluid pockets in a partially treated laminated composite MR fluid sandwich plates are identified to yield the maximum natural frequencies and loss factor. An optimization problem is formulated to identify the optimal location of MR fluid pocket in a laminated composite sandwich plate to maximize the natural frequencies and loss factors, at individual and combination of modes of transverse vibration. The optimization problem is solved using Genetic Algorithm (GA) combined with the finite element formulation developed for a partially treated laminated composite MR fluid sandwich plate. The validity and effectiveness of GA in capturing the optimal locations of MR fluid pockets to maximize the natural frequencies is demonstrated by comparing the results with those obtained using experimental measurements. Furthermore, the optimal locations of the MR fluid treatments are identified to maximize the natural frequencies and loss factors, either individually or combined, under various boundary conditions.

2. Finite element modeling of a partially treated laminated composite MR fluid sandwich plate

A partially treated laminated composite sandwich plate comprising MR fluid (MRF) and rubber segments as core layer (Fig. 1), reported in Manoharan *et al.* (2014b), is considered for the development of the optimization problem and identification of optimal location of MR fluid segments. The equivalent single layer theory is implemented to model the top and bottom composite layers (Fig. 1(a)) of the MR fluid composite sandwich plate. The composite faces are considered to be thin compared to the length and width of the laminate. Hence, Kirchhoff hypothesis in conjunction with the classical laminated plate theory is employed to model the composite face layers. The mid-layer of the partially treated sandwich plate of thickness h_c is composed of identical MR fluid layer segments of length L_p and width B_p at various locations in

association with rubber layers at the remaining locations as shown in Figs. 1(b) and 1(c). Since the Young's moduli of the composite layers are very high compared to MR fluid and the rubber materials, the normal stresses in the middle layer are neglected. Compared to length L and width B of the MR fluid sandwich plate, the face layer thicknesses, h_t and h_b and core layer thickness, h_c are assumed to be very small. The slippage between the composite and core (MR fluid + rubber) layers is also neglected and there is no slippage between the composite face layers. The composite face layers damping and variation in thickness displacement are also negligible. The transverse displacement w is considered to be uniform at any given cross-section of the plate.

2.1 Formulation of the energy equations of a partially treated MR fluid composite sandwich plate

The governing equations of motion of a partially treated MR fluid composite sandwich plate have been formulated using Lagrange's energy approach (Manoharan *et al.* 2014b). To accomplish this, the total strain and kinetic energy of the system are derived.

The strain energy due to top and bottom composite layers, $V_{t,b}$ can be expressed as

$$\begin{aligned}
 V_{t,b} = & \int_0^B \int_0^L \sum_{i=t,b} \left[\frac{1}{2} A_{i11} \left(\frac{\partial u_i}{\partial x} \right)^2 + \frac{1}{2} A_{i22} \left(\frac{\partial v_i}{\partial y} \right)^2 + \frac{1}{2} A_{i66} \left(\frac{\partial u_i}{\partial y} + \frac{\partial v_i}{\partial x} \right)^2 + A_{i12} \left(\frac{\partial u_i}{\partial x} \right) \left(\frac{\partial v_i}{\partial y} \right) \right. \\
 & + A_{i16} \left(\frac{\partial u_i}{\partial y} + \frac{\partial v_i}{\partial x} \right) \left(\frac{\partial u_i}{\partial x} \right) + A_{i26} \left(\frac{\partial u_i}{\partial y} + \frac{\partial v_i}{\partial x} \right) \left(\frac{\partial v_i}{\partial y} \right) - B_{i11} \left(\frac{\partial u_i}{\partial x} \right) \left(\frac{\partial^2 w}{\partial x^2} \right) - B_{i22} \left(\frac{\partial v_i}{\partial y} \right) \left(\frac{\partial^2 w}{\partial y^2} \right) \\
 & - 2B_{i66} \left(\frac{\partial u_i}{\partial y} + \frac{\partial v_i}{\partial x} \right) \left(\frac{\partial^2 w}{\partial x \partial y} \right) - B_{i12} \left(\left(\frac{\partial v_i}{\partial y} \right) \left(\frac{\partial^2 w}{\partial x^2} \right) + \left(\frac{\partial u_i}{\partial x} \right) \left(\frac{\partial^2 w}{\partial y^2} \right) \right) - B_{i16} \left(\frac{\partial u_i}{\partial y} + \frac{\partial v_i}{\partial x} \right) \left(\frac{\partial^2 w}{\partial x^2} \right) \\
 & - B_{i26} \left(\frac{\partial u_i}{\partial y} + \frac{\partial v_i}{\partial x} \right) \left(\frac{\partial^2 w}{\partial y^2} \right) - 2B_{i16} \left(\frac{\partial u_i}{\partial x} \right) \left(\frac{\partial^2 w}{\partial x \partial y} \right) - 2B_{i26} \left(\frac{\partial v_i}{\partial y} \right) \left(\frac{\partial^2 w}{\partial x \partial y} \right) + \frac{1}{2} D_{i11} \left(\frac{\partial^2 w}{\partial x^2} \right)^2 \\
 & + \frac{1}{2} D_{i22} \left(\frac{\partial^2 w}{\partial y^2} \right)^2 + 2D_{i66} \left(\frac{\partial^2 w}{\partial x \partial y} \right)^2 + D_{i12} \left(\frac{\partial^2 w}{\partial x^2} \right) \left(\frac{\partial^2 w}{\partial y^2} \right) + 2D_{i16} \left(\frac{\partial^2 w}{\partial x^2} \right) \left(\frac{\partial^2 w}{\partial x \partial y} \right) \\
 & \left. + 2D_{i26} \left(\frac{\partial^2 w}{\partial y^2} \right) \left(\frac{\partial^2 w}{\partial x \partial y} \right) \right] dx dy \quad (1)
 \end{aligned}$$

where, $A_{ij} = \sum_{k=1}^N Q_{ijk} (z_k - z_{k-1})$; $B_{ij} = \frac{1}{2} \sum_{k=1}^N Q_{ijk} (z_k^2 - z_{k-1}^2)$; $D_{ij} = \frac{1}{3} \sum_{k=1}^N Q_{ijk} (z_k^3 - z_{k-1}^3)$ where z_k the distance of each ply k from the middle plane of the laminate along z direction and N is the number of plies in each laminate.

$[Q_{ij}]$ is the transformed reduced stiffness matrix and its components can be expressed as

$$[Q_{ij}] = [T_1]^{-1} [\bar{Q}_{ij}]_k [T_1]^T \quad (i, j = 1, 2, 6) \quad (2)$$

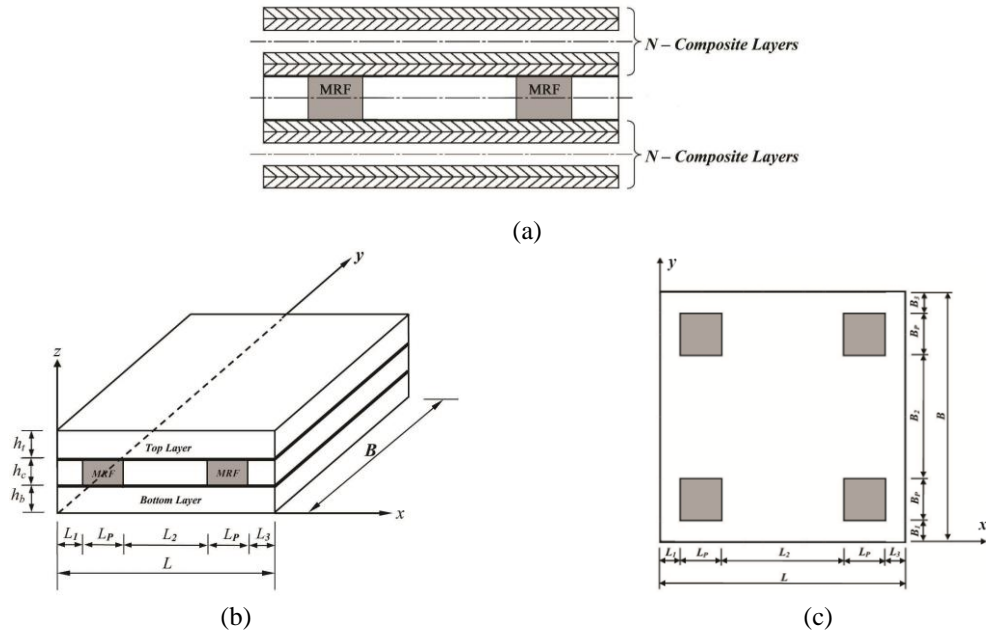


Fig. 1 (a) Representation of a partially treated MR fluid composite sandwich plate with N-number of composite plies, (b) Partially treated MR fluid composite sandwich plate and (c) Schematic top view of core (MR fluid and rubber) layer . (■ - MR fluid, □ - Rubber)

$[T_1]$ is the transformation matrix and can be specified as

$$[T_1] = \begin{bmatrix} \cos^2 \theta & \sin^2 \theta & 2 \cos \theta \sin \theta \\ \sin^2 \theta & \cos^2 \theta & -2 \cos \theta \sin \theta \\ -\cos \theta \sin \theta & \cos \theta \sin \theta & \cos^2 \theta - \sin^2 \theta \end{bmatrix} \quad (3)$$

and $[\bar{Q}_{ij}]_k$ is the constitutive matrix at the lamina level and is given by

$$[\bar{Q}_{ij}]_k = \begin{bmatrix} \bar{Q}_{11} & \bar{Q}_{12} & 0 \\ \bar{Q}_{12} & \bar{Q}_{22} & 0 \\ 0 & 0 & \bar{Q}_{66} \end{bmatrix} \quad (i, j = 1, 2, 6) \quad (4)$$

where $\bar{Q}_{11} = E_1 / (1 - \nu_{12}\nu_{21})$, $\bar{Q}_{12} = \nu_{12}E_2 / (1 - \nu_{12}\nu_{21})$, $\bar{Q}_{22} = E_2 / (1 - \nu_{12}\nu_{21})$, $\bar{Q}_{66} = G_{12}$ and θ is the ply orientation angle, E_1 and E_2 are the Young's moduli of the composite ply along the fiber directions, G_{12} is the shear moduli and ν_{12} and ν_{21} are the Poisson's ratios in material axes.

The strain energy due to core layer (rubber layer + four MR fluid pockets) is presented as

$$V_c = V_{cr} + V_{cf} \quad (5)$$

where V_{cr} is the strain energy of rubber core and V_{cf} is the strain energy of fluid core.

$$\begin{aligned}
V_c = & \frac{1}{2} \int_0^{B_1} \int_0^L (G_r * h_c) \left[\left(\frac{d}{h_c} \left(\frac{\partial w}{\partial x} \right) + \frac{u_t - u_b}{h_c} \right)^2 + \left(\frac{d}{h_c} \left(\frac{\partial w}{\partial y} \right) + \frac{v_t - v_b}{h_c} \right)^2 \right] dx dy \\
& + \frac{1}{2} \int_{B_1}^{B_1+B_p} \int_0^{L_1} (G_r * h_c) \left[\left(\frac{d}{h_c} \left(\frac{\partial w}{\partial x} \right) + \frac{u_t - u_b}{h_c} \right)^2 + \left(\frac{d}{h_c} \left(\frac{\partial w}{\partial y} \right) + \frac{v_t - v_b}{h_c} \right)^2 \right] dx dy \\
& + \frac{1}{2} \int_{B_1}^{B_1+B_p} \int_{L_1}^{L_1+L_p} (G_f * h_c) \left[\left(\frac{d}{h_c} \left(\frac{\partial w}{\partial x} \right) + \frac{u_t - u_b}{h_c} \right)^2 + \left(\frac{d}{h_c} \left(\frac{\partial w}{\partial y} \right) + \frac{v_t - v_b}{h_c} \right)^2 \right] dx dy \\
& + \frac{1}{2} \int_{B_1}^{B_1+B_p} \int_{L_1+L_p}^{L_1+L_p+L_2} (G_r * h_c) \left[\left(\frac{d}{h_c} \left(\frac{\partial w}{\partial x} \right) + \frac{u_t - u_b}{h_c} \right)^2 + \left(\frac{d}{h_c} \left(\frac{\partial w}{\partial y} \right) + \frac{v_t - v_b}{h_c} \right)^2 \right] dx dy \\
& + \frac{1}{2} \int_{B_1}^{B_1+B_p} \int_{L_1+L_p+L_2}^{L_1+2L_p+L_2} (G_f * h_c) \left[\left(\frac{d}{h_c} \left(\frac{\partial w}{\partial x} \right) + \frac{u_t - u_b}{h_c} \right)^2 + \left(\frac{d}{h_c} \left(\frac{\partial w}{\partial y} \right) + \frac{v_t - v_b}{h_c} \right)^2 \right] dx dy \\
& + \frac{1}{2} \int_{B_1}^{B_1+B_p} \int_{L_1+2L_p+L_2}^L (G_r * h_c) \left[\left(\frac{d}{h_c} \left(\frac{\partial w}{\partial x} \right) + \frac{u_t - u_b}{h_c} \right)^2 + \left(\frac{d}{h_c} \left(\frac{\partial w}{\partial y} \right) + \frac{v_t - v_b}{h_c} \right)^2 \right] dx dy \\
& + \frac{1}{2} \int_{B_1+B_p}^{B_1+B_p+B_2} \int_0^L (G_r * h_c) \left[\left(\frac{d}{h_c} \left(\frac{\partial w}{\partial x} \right) + \frac{u_t - u_b}{h_c} \right)^2 + \left(\frac{d}{h_c} \left(\frac{\partial w}{\partial y} \right) + \frac{v_t - v_b}{h_c} \right)^2 \right] dx dy \\
& + \frac{1}{2} \int_{B_1+B_p+B_2}^{B_1+2B_p+B_2} \int_0^{L_1} (G_r * h_c) \left[\left(\frac{d}{h_c} \left(\frac{\partial w}{\partial x} \right) + \frac{u_t - u_b}{h_c} \right)^2 + \left(\frac{d}{h_c} \left(\frac{\partial w}{\partial y} \right) + \frac{v_t - v_b}{h_c} \right)^2 \right] dx dy \\
& + \frac{1}{2} \int_{B_1+B_p+B_2}^{B_1+2B_p+B_2} \int_{L_1}^{L_1+L_p} (G_f * h_c) \left[\left(\frac{d}{h_c} \left(\frac{\partial w}{\partial x} \right) + \frac{u_t - u_b}{h_c} \right)^2 + \left(\frac{d}{h_c} \left(\frac{\partial w}{\partial y} \right) + \frac{v_t - v_b}{h_c} \right)^2 \right] dx dy \\
& + \frac{1}{2} \int_{B_1+B_p+B_2}^{B_1+2B_p+B_2} \int_{L_1+L_p}^{L_1+L_p+L_2} (G_r * h_c) \left[\left(\frac{d}{h_c} \left(\frac{\partial w}{\partial x} \right) + \frac{u_t - u_b}{h_c} \right)^2 + \left(\frac{d}{h_c} \left(\frac{\partial w}{\partial y} \right) + \frac{v_t - v_b}{h_c} \right)^2 \right] dx dy \\
& + \frac{1}{2} \int_{B_1+B_p+B_2}^{B_1+2B_p+B_2} \int_{L_1+L_p+L_2}^{L_1+2L_p+L_2} (G_f * h_c) \left[\left(\frac{d}{h_c} \left(\frac{\partial w}{\partial x} \right) + \frac{u_t - u_b}{h_c} \right)^2 + \left(\frac{d}{h_c} \left(\frac{\partial w}{\partial y} \right) + \frac{v_t - v_b}{h_c} \right)^2 \right] dx dy \\
& + \frac{1}{2} \int_{B_1+B_p+B_2}^{B_1+2B_p+B_2} \int_{L_1+2L_p+L_2}^L (G_r * h_c) \left[\left(\frac{d}{h_c} \left(\frac{\partial w}{\partial x} \right) + \frac{u_t - u_b}{h_c} \right)^2 + \left(\frac{d}{h_c} \left(\frac{\partial w}{\partial y} \right) + \frac{v_t - v_b}{h_c} \right)^2 \right] dx dy \\
& + \frac{1}{2} \int_{B_1+2B_p+B_2}^B \int_0^L (G_r * h_c) \left[\left(\frac{d}{h_c} \left(\frac{\partial w}{\partial x} \right) + \frac{u_t - u_b}{h_c} \right)^2 + \left(\frac{d}{h_c} \left(\frac{\partial w}{\partial y} \right) + \frac{v_t - v_b}{h_c} \right)^2 \right] dx dy
\end{aligned} \tag{6}$$

where $d = \frac{h_t}{2} + h_c + \frac{h_b}{2}$ and G_r and G_f are the shear modulus of the rubber and MR fluid respectively. The complex shear modulus of MR fluid (G_f) can be expressed as, $G_f = G' + jG''$ where G' is the storage modulus and G'' is the loss modulus of MR fluid.

Therefore the strain energy of the composite sandwich plate, V can be expressed as

$$V = V_{t,b} + V_c \quad (7)$$

where L and B are the length and width of the plate in x and y directions in composite sandwich plate, respectively.

The total kinetic energy of the MR fluid composite sandwich plate consists of the kinetic energy associated with i) the axial deformations of the composite layers (T_1); ii) the transverse motion of the composite layers, rubber layer and the MR layers (T_2); iii) the rotational deformation of the MR layer and rubber layer due to the strain displacements (T_3).

The kinetic energy associated with the axial deformations of the laminated composite layers (T_1) can be expressed as

$$T_1 = \frac{1}{2} \int_0^B \int_0^L \left[\rho_t h_t \left(\left(\frac{\partial u_t}{\partial t} \right)^2 + \left(\frac{\partial v_t}{\partial t} \right)^2 \right) + \rho_b h_b \left(\left(\frac{\partial u_b}{\partial t} \right)^2 + \left(\frac{\partial v_b}{\partial t} \right)^2 \right) \right] dx dy \quad (8)$$

The kinetic energy associated with the transverse motion of the laminated composite layers, rubber layer and MR fluid layer (T_2) can be expressed as

$$\begin{aligned} T_2 = & \frac{1}{2} \int_0^B \int_0^L \left[(\rho_t h_t + \rho_b h_b) \left(\frac{\partial w}{\partial t} \right)^2 \right] dx dy + \frac{1}{2} \int_0^{B_1} \int_0^{L_1} \left[(\rho_{cr} h_c) \left(\frac{\partial w}{\partial t} \right)^2 \right] dx dy \\ & + \frac{1}{2} \int_{B_1}^{B_1+B_p} \int_0^{L_1} \left[(\rho_{cr} h_c) \left(\frac{\partial w}{\partial t} \right)^2 \right] dx dy + \frac{1}{2} \int_{B_1}^{B_1+B_p} \int_{L_1}^{L_1+L_p} \left[(\rho_{cf} h_c) \left(\frac{\partial w}{\partial t} \right)^2 \right] dx dy \\ & + \frac{1}{2} \int_{B_1}^{B_1+B_p} \int_{L_1+L_p}^{L_1+L_p+L_2} \left[(\rho_{cr} h_c) \left(\frac{\partial w}{\partial t} \right)^2 \right] dx dy + \frac{1}{2} \int_{B_1}^{B_1+B_p} \int_{L_1+L_p+L_2}^{L_1+2L_p+L_2} \left[(\rho_{cf} h_c) \left(\frac{\partial w}{\partial t} \right)^2 \right] dx dy \\ & + \frac{1}{2} \int_{B_1}^{B_1+B_p} \int_{L_1+2L_p+L_2}^{L_1+2L_p+L_2+L_2} \left[(\rho_{cr} h_c) \left(\frac{\partial w}{\partial t} \right)^2 \right] dx dy + \frac{1}{2} \int_{B_1+B_p}^{B_1+B_p+B_2} \int_0^{L_1} \left[(\rho_{cr} h_c) \left(\frac{\partial w}{\partial t} \right)^2 \right] dx dy \\ & + \frac{1}{2} \int_{B_1+B_p+B_2}^{B_1+2B_p+B_2} \int_0^{L_1} \left[(\rho_{cr} h_c) \left(\frac{\partial w}{\partial t} \right)^2 \right] dx dy + \frac{1}{2} \int_{B_1+B_p+B_2}^{B_1+2B_p+B_2} \int_{L_1}^{L_1+L_p} \left[(\rho_{cf} h_c) \left(\frac{\partial w}{\partial t} \right)^2 \right] dx dy \\ & + \frac{1}{2} \int_{B_1+B_p+B_2}^{B_1+2B_p+B_2} \int_{L_1+L_p}^{L_1+L_p+L_2} \left[(\rho_{cr} h_c) \left(\frac{\partial w}{\partial t} \right)^2 \right] dx dy + \frac{1}{2} \int_{B_1+B_p+B_2}^{B_1+2B_p+B_2} \int_{L_1+L_p+L_2}^{L_1+2L_p+L_2} \left[(\rho_{cf} h_c) \left(\frac{\partial w}{\partial t} \right)^2 \right] dx dy \\ & + \frac{1}{2} \int_{B_1+B_p+B_2}^{B_1+2B_p+B_2} \int_{L_1+2L_p+L_2}^{L_1+2L_p+L_2+L_2} \left[(\rho_{cr} h_c) \left(\frac{\partial w}{\partial t} \right)^2 \right] dx dy + \frac{1}{2} \int_{B_1+2B_p+B_2}^{B_1+2B_p+B_2+B_2} \int_0^{L_1} \left[(\rho_{cr} h_c) \left(\frac{\partial w}{\partial t} \right)^2 \right] dx dy \end{aligned} \quad (9)$$

The kinetic energy associated with the rotational deformation of the rubber layer and MR fluid layer (T_3) can be expressed as

(10)

$$\begin{aligned}
& + \frac{1}{2} \int_{B_1+B_p+B_2}^{B_1+2B_p+B_2} \int_{L_1+2L_p+L_2}^L \rho_{cr} I_{cr} \left[\left(\frac{d}{h_c} \left(\frac{\partial^2 w}{\partial x \partial t} \right) + \left(\frac{\frac{\partial u_t}{\partial t} - \frac{\partial u_b}{\partial t}}{h_c} \right) \right)^2 + \left(\frac{d}{h_c} \left(\frac{\partial^2 w}{\partial y \partial t} \right) + \left(\frac{\frac{\partial v_t}{\partial t} - \frac{\partial v_b}{\partial t}}{h_c} \right) \right)^2 \right] dx dy \\
& + \frac{1}{2} \int_{B_1+2B_p+B_2}^B \int_0^L \rho_{cr} I_{cr} \left[\left(\frac{d}{h_c} \left(\frac{\partial^2 w}{\partial x \partial t} \right) + \left(\frac{\frac{\partial u_t}{\partial t} - \frac{\partial u_b}{\partial t}}{h_c} \right) \right)^2 + \left(\frac{d}{h_c} \left(\frac{\partial^2 w}{\partial y \partial t} \right) + \left(\frac{\frac{\partial v_t}{\partial t} - \frac{\partial v_b}{\partial t}}{h_c} \right) \right)^2 \right] dx dy
\end{aligned}$$

where ρ_t and ρ_b are the mass densities of the top and bottom composite layers, and ρ_{cf} and ρ_{cr} are the mass densities of the MR fluid and the rubber materials, respectively. I_{cf} and I_{cr} are the second moment of inertia with respect to the centroid of the MR fluid layer and the rubber materials, respectively.

The total kinetic energy of the MR fluid composite sandwich plate can thus be obtained as

$$T = T_1 + T_2 + T_3 \quad (11)$$

2.2 Finite element formulation

In the finite element formulation, a rectangular plate element with four nodes and seven degrees of freedom (DOF) per node is considered for the analysis. The various DOFs considered at each node of the rectangular element are u_t , u_b , v_t , v_b , w , θ_x and θ_y . u_t and u_b are considered as the in-plane displacements of top and bottom composite layers in x direction, respectively and v_t and v_b are considered as the in-plane displacements of the top and bottom layers in y direction, respectively while w is considered as the transverse displacement of the sandwich plate, and θ_x and θ_y are the rotational displacements with respect to x -and y direction of the sandwich plate, respectively. The in-plane and transverse displacements are presented as

$$\begin{aligned}
w_j(x, y, t) &= N_{wj}(x, y)q(t) & j &= 1, 2, 3, 4 \\
u_{ij}(x, y, t) &= N_{uij}(x, y)q(t), & i &= t, b; j = 1, 2, 3, 4 \\
v_{ij}(x, y, t) &= N_{vij}(x, y)q(t), & i &= t, b; j = 1, 2, 3, 4
\end{aligned} \quad (12)$$

where, $q(t) = [u_t, v_t, u_b, v_b, w, \theta_x, \theta_y]^T$, $N_w(x, y)$, $N_{ui}(x, y)$ and $N_{vi}(x, y)$ are the shape functions of the plate element and are presented in Appendix. Lagrange's equations are used to develop the governing differential equations in finite element form.

Assembling the mass and stiffness matrices and the force vector for all the elements yields the system of governing equations of motion of the MR composite sandwich plate in the finite element form, which can be expressed in the following general form

$$[M]\{\ddot{d}\} + [K]\{d\} = \{F\} \quad (13)$$

where $[M]$, $[K]$ and $\{F\}$ are the system mass and stiffness matrices and the force vector, respectively.

3. Formulation of the optimization problem and solution methodology

The finite element formulation developed for a partially treated MR fluid composite sandwich plate in section 2 is used here to formulate the fitness function. The objectives are to identify the optimal location of MR fluid pockets for achieving the maximum natural frequencies and loss factors at individual and combination of transverse modes. The loss factor of the laminated composite MR fluid sandwich plate is derived as the ratio of the square of the imaginary component of the complex natural frequency to that of the real component (Yalcintas and Dai 2004, Yeh and Shih 2006). The loss factor is merely the ratio of energy dissipated per radian to the total strain energy V , both of which increase with the magnetic field. The objective criterion is formulated by considering a partially treated MR fluid composite sandwich plate, as presented in Fig. 1(c). As the first few modes are important in structural vibration, the first five modes of vibration are considered here. The optimization process is carried for four different cases under the various boundary conditions such as clamped (C), simply supported (S) and free (F) along the edges of the plate including CCCC, SSSS, CFCF, SFSF and CFFF and specified starting from the left end of the sandwich plate in counter clockwise direction. The various optimization problems are formulated as follows:

Case 1: The objective function is formulated to seek the optimal locations of MR fluid pockets to yield the maximum fundamental natural frequency. Then the objective function for Case 1 can be specified such that

$$\text{Maximize } f(X) = \omega_1 \quad (14)$$

Subject to: $0 < X \leq N$, where N is the number of finite elements of the sandwich plate and X defines the location of MR fluid pockets in the sandwich plate, such that $X = \{(x_1, y_1), (x_2, y_2), (x_3, y_3), (x_4, y_4)\}$ specified with starting coordinates of MR fluid pockets with length L_p and width B_p , and ω_1 is the fundamental natural frequency.

Case 2: The objective function is formulated to seek the optimal locations of MR fluid pockets to achieve maximum fundamental loss factor. The objective function for Case 2 is such that

$$\text{Maximize } f(X) = \eta_1 \quad (15)$$

Subject to: $0 < X \leq N$, where η_1 is the fundamental loss factor

Case 3: The objective function is formulated to seek the optimal locations of MR fluid pockets to maximize the linear combination of the fundamental natural frequency and the fundamental loss factor. Hence, the objective function for Case 3 is

$$\text{Maximize } f(X) = \alpha_1 \omega_1 + \alpha_2 \eta_1 \quad (16)$$

Subject to: $0 < X \leq N$, where α_1 and α_2 are the weightage factors ranging from 0 to 1 such that $\alpha_1 + \alpha_2 = 1$, ω_1 and η_1 are the fundamental natural frequency and fundamental loss factor of the sandwich plate.

Case 4: The objective function is formulated to seek the optimal locations of MR fluid pockets to maximize the linear combination of summation of the first five modes of natural frequencies and loss factors. The objective function for Case 4 is

$$\text{Maximize } f(X) = \alpha_1 \sum_{i=1}^5 \omega_i + \alpha_2 \sum_{i=1}^5 \eta_i \quad (17)$$

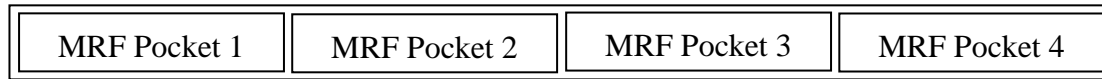


Fig. 2 Chromosome structure for a partially treated laminated composite MR fluid sandwich plate

Subject to: $0 < x \leq N$, where α_1 and α_2 are the weightage factors ranging from 0 to 1 such that $\alpha_1 + \alpha_2 = 1$ and $i = 1, 2, \dots, 5$, ω_i and η_i are the natural frequency and loss factor at corresponding first five modes.

Genetic Algorithm is used to identify the optimal locations of MR fluid pockets in a partially treated laminated composite MR fluid sandwich plate that yield maximum natural frequency and loss factor. A partially treated MR fluid composite sandwich plate is considered as one chromosome. Each MR fluid pocket in a composite sandwich plate is considered as a substring. So each chromosome contains four substrings as shown in Fig. 2. The flow chart shown in Fig. 3 provides the detailed operational process of GA in identifying the optimal location of MR pockets in the partially treated laminated composite MR fluid sandwich plate.

4. Results and discussions

The validity of the proposed finite element formulation coupled with the genetic algorithm in identifying the optimal locations of MR fluid pockets in a partially treated MR fluid composite sandwich plate is demonstrated by comparing the results obtained through laboratory experiments on a prototype MR fluid sandwich plate. The present FEA coupled with GA is used to solve the optimization problems formulated in section 3 by generating the codes in MATLAB by following the steps involved in Fig. 3. The simulation is performed on Case 1 in which the locations of MR fluid pockets are identified to maximize the fundamental natural frequency of the partially treated MR fluid sandwich plate. A prototype partially treated MR fluid composite sandwich plate was fabricated by locating the MR fluid pockets in identical locations obtained using the present FEA coupled with GA and the results are compared. The following material and geometrical properties were considered for the simulation: $h_t = h_b = 1.5 \text{ mm}$; $h_c = 1.5 \text{ mm}$; $\rho_t = \rho_b = 1779.34 \text{ kg/m}^3$; $\rho_{cf} = 2812 \text{ kg/m}^3$; $\rho_{cr} = 910 \text{ kg/m}^3$; $E_1 = 31.446 \text{ GPa}$; $E_2 = 7.435 \text{ GPa}$; $\nu_{12} = 0.2424$; $\nu_{21} = 0.0646$; $G_{12} = 2.887 \text{ GPa}$; The variation of shear modulus (G') and loss modulus (G'') with respect to the magnetic field intensity is considered as (Manoharan *et al.* 2014b).

$$\begin{aligned}
 G' &= -0.05035 G^2 + 428.355 G + 858.8 \\
 G'' &= -0.057 G^2 + 452.105 G + 848.35
 \end{aligned}
 \tag{18}$$

where G is the magnetic field intensity in Gauss.

A partially treated laminated composite MR fluid sandwich plate clamped at right and left ends and free at the other ends (CFCF) was fabricated using two thin glass fiber laminated strips of $300 \text{ mm} \times 300 \text{ mm} \times 1.6 \text{ mm}$. The top and bottom composite laminated plates were fabricated using a hand-layup technique. Each laminate consists of seven laminas with fiber angle orientation

of $[0^\circ/90^\circ/0^\circ/90^\circ]$, E-glass unidirectional fibers. Epoxy resins (LY0556) were applied to dry plies after laid-up is completed in between all the plies.

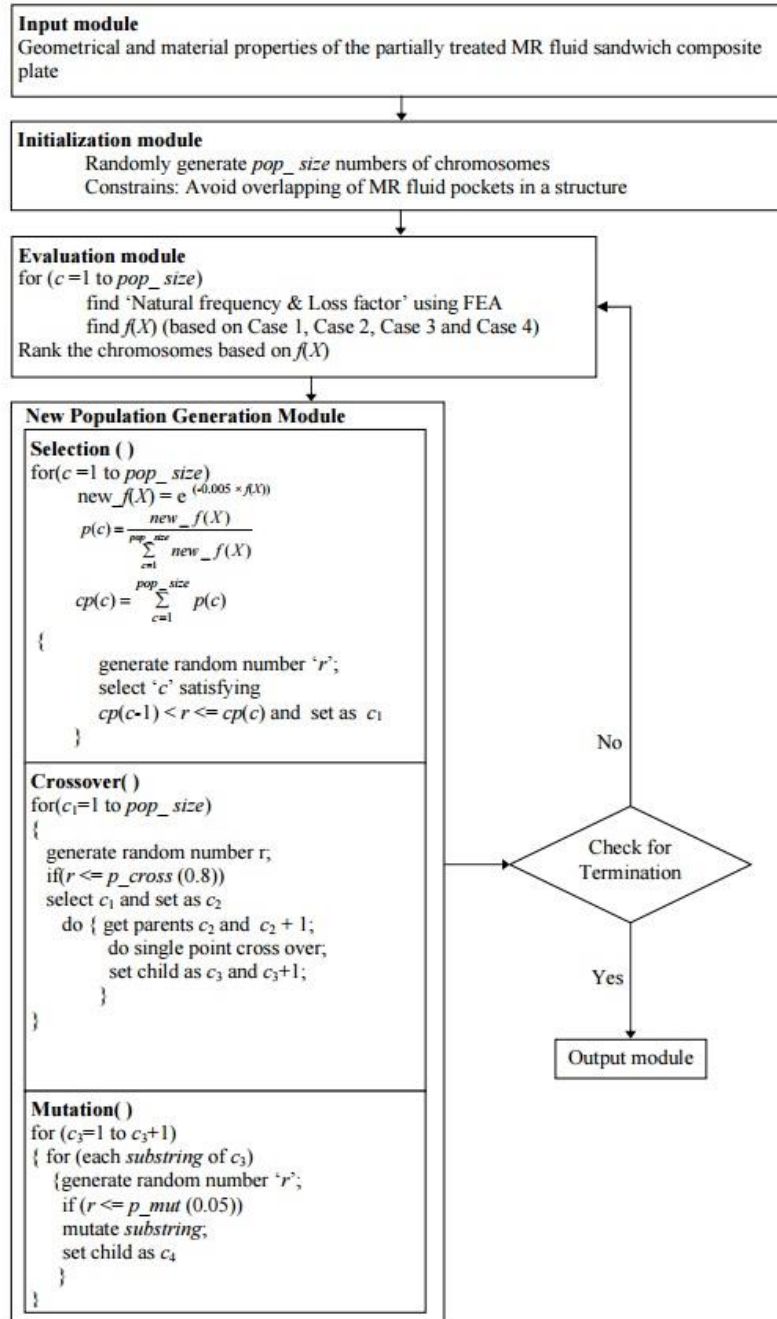


Fig. 3 Block diagram of GA to search optimal location of MR fluid Pockets

A vacuum bag with breather assemblies was placed over the layup in order to remove the excess resin through vacuum pump from the laminated plate and then it was cured in an autoclave at 100°C to increase strength of laminated plate. The proper volume fraction was maintained throughout the manufacturing process to achieve the better mechanical properties of the composite plate.

Two laminated composite plates of $([0^\circ/90^\circ/0^\circ/90^\circ]_s)$ and $[0^\circ/90^\circ/0^\circ/90^\circ]_s$, respectively were arranged to create a uniform gap of 1mm to fill MR fluid (MRHCCS4-B). The MR fluid was filled only at the mid-layer of the sandwich plate with four segments of 50 mm x 50 mm x 1 mm at identical locations obtained from the simulations. The coordinates $P_i(x,y)$, $i = 1, 2, 3$ and 4 at the starting point of each MR fluid pockets are $P_1(75,75)$, $P_2(250,25)$, $P_3(250,175)$ and $P_4(50,175)$ as shown in Fig. 4. The dark area shows the location of MR fluid. The high strength natural rubber (1mm thickness) is considered to be filled at the remaining locations in order to maintain the uniform gap between two laminates. The final configuration of sandwich plate is obtained as $([0^\circ/90^\circ/0^\circ/90^\circ]_s/\text{core layer}/[0^\circ/90^\circ/0^\circ/90^\circ]_s)$.

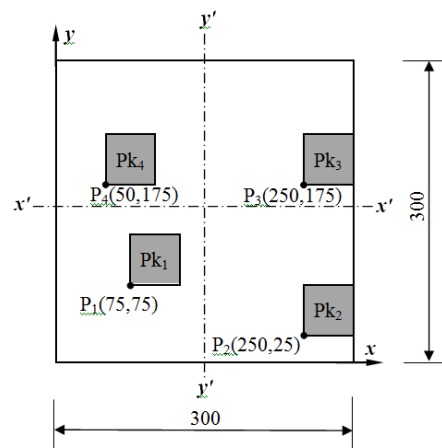


Fig. 4 Representation of the optimal locations of MR fluid in the middle layer of a partially treated MR fluid composite sandwich plate identified in Case I at zero magnetic field. [All dimensions are in mm]

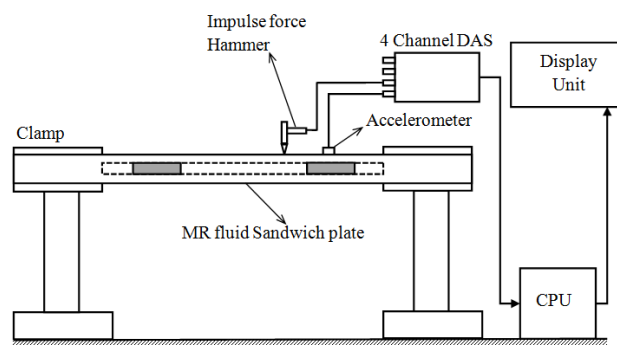


Fig. 5 Block diagram of the experimental setup of a partially treated laminated composite MR fluid sandwich plate

Table 1 Comparison on natural frequencies at optimal layout of a partially treated cantilever laminated composite MR fluid sandwich plate identified through GA coupled the finite-element formulations with the experimental measured frequencies at zero magnetic field

Mode	Natural frequencies (Hz)		% deviation
	Measured	GA coupled with FEM	
1	131.56	141.18	6.8
2	150.81	154.14	2.1
3	243.87	230.15	5.6

Table 2 Effect of magnetic field on the variation of natural frequency of the partially treated MR fluid sandwich plate

Magnetic fields (Gauss)	Mode	Natural frequencies (Hz)
0 G	1	141.18
	2	154.14
	3	230.15
250 G	1	141.25
	2	154.19
	3	230.20
500 G	1	141.32
	2	154.23
	3	230.25

The partially treated laminated composite MR fluid sandwich plate was clamped (CFCF) at the left and right edges using a steel fixture. Fig. 5 shows the schematic diagram of the experimental set-up. The impulse hammer (Impulse Force Hammer-086C03) was used to excite the sandwich plate and the acceleration signal was measured by a single axis accelerometer. This acceleration signals were then converted into frequency response function using 4 channel Data Acquisition System (Model No. ATA-DAQ042451). The natural frequencies of the MR fluid sandwich plate were measured at various modes free vibration responses under zero magnetic field intensities.

Table 1 shows the comparisons of the first three natural frequencies identified through genetic algorithm coupled with finite element formulation with those obtained experimentally under zero magnetic field intensity. A very good agreement could be observed between the computed and measured frequencies, irrespective of the mode of vibration. The reason for the deviation between the results evaluated using FEM and experimental tests could be related to the practical reasons including the fabrication of laminated composite plates using hand layup technique and creation of partially treated MR fluid segments in the middle layer of sandwich plate.

As the size of MR fluid sandwich plate is large and unavailability of the permanent magnets to

generate the magnetic field over the surface of large size, the results evaluated using FEM were validated with those obtained experimentally without applying magnetic field. Further, the effect of magnetic field on the variation of natural frequencies of the partially treated MR fluid sandwich structures has been already demonstrated in (Rajamohan *et al.* 2010b, Manoharan *et al.* 2014b). However the variation of natural frequency of the partially treated MR fluid composite sandwich plate with applied magnetic field is studied using FEM and the results are presented in Table 2 for higher magnetic field. It can be seen that the natural frequency increases with increase in magnetic field at all the modes considered. The reason for the minimal variation is due to smaller size of MR fluid pockets located in the partially treated MR fluid sandwich plate. Similar variation was also observed in (Rajamohan *et al.* 2010b, Manoharan *et al.* 2014b).

The optimal locations of MR fluid pockets were identified for the four cases of optimization problems. In Case 1 and Case 2 of the optimization problems, the whole weightage has given to yield the maximization of fundamental natural frequency and fundamental loss factor, respectively. In Case 3 and Case 4 of the optimization problems, the weightage factors α_1 and α_2 are considered as 0.5 to provide the equal weightage for both natural frequencies and loss factors. Tables 3-6 show the optimized locations of MR fluid pockets and the corresponding first five natural frequencies and loss factors of the partially treated laminated composite MR fluid sandwich plate for various boundary conditions at a magnetic fields of 500 Gauss identified by solving the optimization problems presented in Cases 1 - 4, respectively. The coordinates $P_i(x,y)$, $i = 1, 2, 3$ and 4 are the starting points of each MR fluid pockets. The dark area shows the location of MR fluid and the high strength natural rubber is considered to be filled at the remaining locations. From the tabulated results, it can be understood that the optimal locations of MR fluid pockets strongly influence the natural frequencies and loss factors of the sandwich plate, irrespective of the boundary conditions and objective functions.

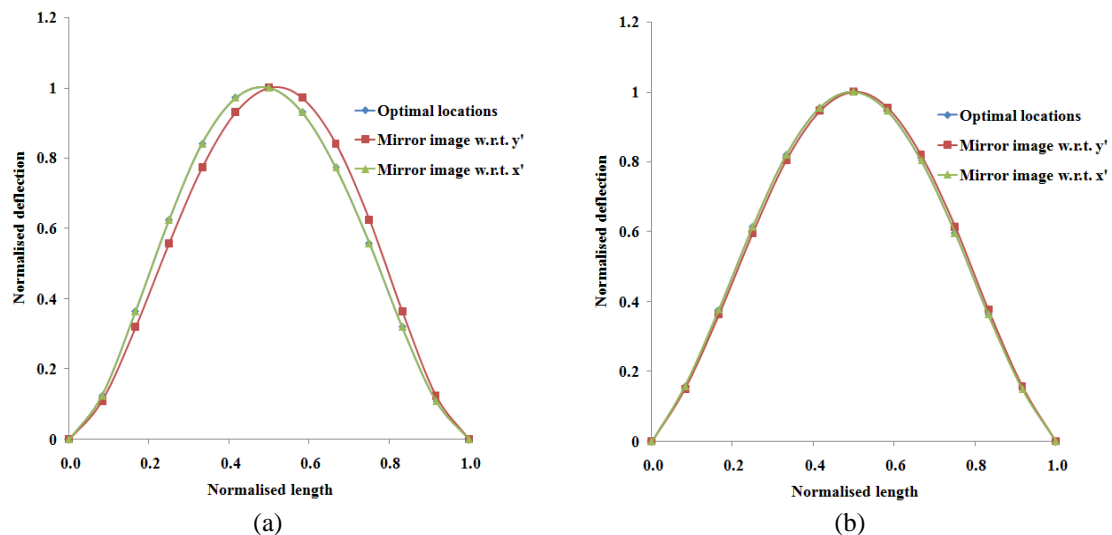


Fig. 6 Comparison of the fundamental mode shape of an optimal layout of a partially treated laminated composite MR fluid sandwich plate with the location of MR fluid pockets in the regions of mirror image with respect to geometrical centre line x' and y' axes under (a) CCCC and (b) SSSS end conditions

The simulations are also performed to investigate the natural frequency and loss factor by locating MR fluid pockets in the regions of mirror image of the optimal locations with respect to the geometrical centre lines parallel to x - axis ($x'x'$) and y - axis ($y'y'$) of the sandwich plate [Fig. 4], under various boundary conditions for all cases. It is found that the natural frequencies and loss factors are identical under symmetric boundary conditions such as CCCC, SSSS, CFCF and SFSF. However, similar observations could not be seen under unsymmetric boundary conditions such as CFFF. Further, even though the magnitude of natural frequencies and loss factors are identical at regions identified through GA and mirror image with respect to geometrical centre lines, the peak deflection in the mode shapes are shifted due to change in location of MR fluid pockets under all the cases as presented in Fig. 6. It can also be observed that CCCC end condition yields the highest natural frequency and loss factor while CFFF end condition yields the lowest natural frequency and loss factor at a applied magnetic field 500 G. Due to the flexibility of the end conditions, CCCC and CFFF yield, respectively, the highest and lowest stiffness of the structures with identical mass. Hence, the natural frequencies and loss factors of the sandwich plate under CCCC end conditions are higher than those with CFFF end conditions.

It can also be noted from Table 3 that the MR fluid treatments near the support would yield higher fundamental natural frequency for symmetric boundary conditions such as CCCC, SSSS, CFCF and SFSF. It is also observed in such cases that the solutions of the optimization problem converged towards relatively greater distribution of MR fluids. This can be associated with greatest stiffness of the structure with symmetric end conditions, which would require larger distribution of MR fluid pockets. However, similar variations could not be observed under CFFF end conditions where the solutions of the optimization problem converged towards relatively greater clustering of MR fluid segments nearer to the fixed ends. This can also be associated with yielding highest stiffness where the MR fluid segments are located nearer to the constraint end.

The results from Table 4 suggests that the optimization problem to maximize the fundamental loss factor converged towards greater clustering of MR fluid segments nearer to constraint ends under CCCC, SSSS, CFCF and SFSF rather than relatively greater distribution manner as presented in Table 3 for maximization of fundamental natural frequency [Case-1]. As it is known that the loss factor is merely a ratio of the energy dissipated per radian to the total strain energy, greater clustering of MR fluid nearer to constraints yields higher dissipated energy and leads to higher loss factors. However, similar observations could not be seen in CFFF end conditions where the clustering of MR fluid nearer to the free end yields higher loss factor. This can also be associated that greater clustering of MR fluid nearer to the unconstraint ends.

Table 5 summarizes the optimal layout obtained to maximize the summation of fundamental natural frequency and loss factor with identical weightage. The results consistently show that the optimal locations of MR fluid segments derived from the consideration of linear combination of the fundamental natural frequency and loss factor are much similar to those identified for fundamental natural frequency in such a way that the MR fluid segments are distributed relatively among the regions under CCCC, SSSS, CFCF and SFSF end conditions while they are located relatively greater clustering under CFFF end conditions. This can be associated with the convergence towards the fundamental natural frequency.

Table 6 summarizes the optimal layout obtained to maximize the linear combination of summation of the first fives of natural frequencies and loss factors. The results consistently show that the optimal locations of MR fluid segments derived from Case (4) are much similar to those identified for maximization of fundamental loss factor [Case 2] in such a way that the locations of MR fluid segments are converged towards greater clustering nearer to the constraint ends. This

can be associated with the convergence towards the fundamental loss factor.

Table 3 Optimal location of MR fluid pockets in a partially treated laminated composite MR fluid sandwich plate under various end conditions at a magnetic field of 500 G identified using GA as in Case – 1 [Maximization of fundamental natural frequency]

Boundary condition	Optimal configuration and co-ordinates of MR fluid pockets location	Mode Nos.	Natural frequency (Hz)	Loss factor
CCCC		1	231.07	0.0003
		2	408.95	0.0017
		3	433.46	0.0005
		4	529.18	0.0032
		5	663.77	0.0024
SSSS		1	218.73	0.0011
		2	367.47	0.0062
		3	390.45	0.0025
		4	473.37	0.0046
		5	546.04	0.0075
CFCF		1	156.42	0.0018
		2	172.58	0.0008
		3	254.74	0.0010
		4	361.11	0.0030
		5	393.95	0.0019
SFSF		1	147.54	0.0012
		2	163.19	0.0007
		3	246.05	0.0008
		4	351.75	0.0010
		5	375.12	0.0006
CFFF		1	29.38	0.0003
		2	49.97	0.0001
		3	158.04	0.0017
		4	181.75	0.0002
		5	194.05	0.0005

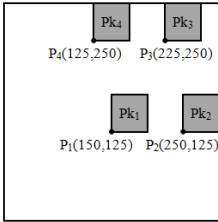
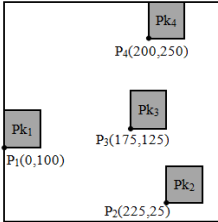
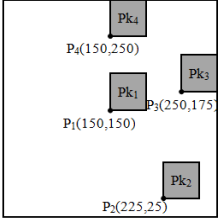
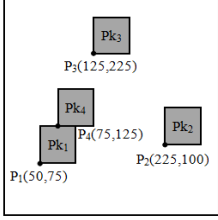
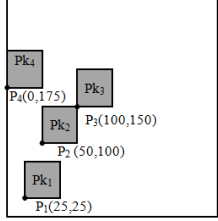
Table 4 Optimal location of MR fluid pockets in a partially treated laminated composite MR fluid sandwich plate under various end conditions at a magnetic field of 500 G identified using GA as in Case 2 [Maximization of fundamental loss factor]

Boundary condition	Optimal configuration and co-ordinates of MR fluid pockets location	Mode Nos.	Natural frequency (Hz)	Loss factor
CCCC	<p>Diagram showing optimal MR fluid pocket locations for CCCC boundary condition. The plate is a square with four corners labeled Pk1, Pk2, Pk3, and Pk4. Pk1 is at (75, 125), Pk2 is at (150, 200), Pk3 is at (75, 250), and Pk4 is at (0, 200).</p>	1	207.92	0.0037
		2	361.15	0.0059
		3	391.37	0.0033
		4	503.07	0.0056
		5	608.45	0.0051
SSSS	<p>Diagram showing optimal MR fluid pocket locations for SSSS boundary condition. The plate is a square with four corners labeled Pk1, Pk2, Pk3, and Pk4. Pk1 is at (100, 25), Pk2 is at (250, 0), Pk3 is at (250, 100), and Pk4 is at (75, 225).</p>	1	201.36	0.0066
		2	320.34	0.0111
		3	379.41	0.0030
		4	471.30	0.0041
		5	553.60	0.0067
CFCF	<p>Diagram showing optimal MR fluid pocket locations for CFCF boundary condition. The plate is a square with four corners labeled Pk1, Pk2, Pk3, and Pk4. Pk1 is at (50, 50), Pk2 is at (125, 100), Pk3 is at (125, 250), and Pk4 is at (0, 250).</p>	1	141.73	0.0082
		2	170.34	0.0007
		3	249.36	0.0022
		4	320.71	0.0090
		5	401.36	0.0016
SFSF	<p>Diagram showing optimal MR fluid pocket locations for SFSF boundary condition. The plate is a square with four corners labeled Pk1, Pk2, Pk3, and Pk4. Pk1 is at (125, 0), Pk2 is at (250, 50), Pk3 is at (225, 150), and Pk4 is at (50, 250).</p>	1	121.85	0.0265
		2	148.38	0.0047
		3	230.11	0.0065
		4	288.98	0.0094
		5	343.34	0.0031
CFFF	<p>Diagram showing optimal MR fluid pocket locations for CFFF boundary condition. The plate is a square with four corners labeled Pk1, Pk2, Pk3, and Pk4. Pk1 is at (125, 0), Pk2 is at (250, 175), Pk3 is at (175, 250), and Pk4 is at (100, 250).</p>	1	28.25	0.0011
		2	45.58	0.0049
		3	151.09	0.0026
		4	175.48	0.0034
		5	179.95	0.0014

Table 5 Optimal location of MR fluid pockets in a partially treated laminated composite MR fluid sandwich plate under various end conditions at a magnetic field of 500 G identified using GA as in Case 3. [Maximization of summation of 50 % of fundamental natural frequency and 50 % of fundamental loss factor]

Boundary condition	Optimal configuration and co-ordinates of MR fluid pockets location	Mode Nos.	Natural frequency (Hz)	Loss factor
CCCC		1	218.88	0.0008
		2	344.28	0.0012
		3	427.67	0.0024
		4	505.19	0.0019
		5	550.74	0.0020
SSSS		1	214.73	0.0008
		2	365.77	0.0022
		3	398.16	0.0019
		4	485.47	0.0039
		5	572.68	0.0057
CFCF		1	156.24	0.0008
		2	170.49	0.0003
		3	255.01	0.0012
		4	372.05	0.0024
		5	400.56	0.0012
SFSF		1	99.97	0.0008
		2	122.47	0.0006
		3	247.92	0.0026
		4	254.83	0.0037
		5	282.31	0.0050
CFFF		1	17.46	0.0002
		2	45.16	0.0003
		3	102.03	0.0010
		4	149.26	0.0010
		5	218.72	0.0006

Table 6 Optimal location of MR fluid pockets in a partially treated laminated composite MR fluid sandwich plate under various end conditions at a magnetic field of 500 G identified using GA as in Case 4. [Maximization of the linear combination of summation of the first five modes of natural frequencies and loss factors]

Boundary condition	Optimal configuration and co-ordinates of MR fluid pockets location	Mode Nos.	Natural frequency (Hz)	Loss factor
CCCC		1	214.75	0.0013
		2	383.43	0.0031
		3	404.21	0.0026
		4	556.91	0.0012
		5	608.33	0.0028
SSSS		1	208.49	0.0015
		2	366.86	0.0031
		3	376.98	0.0025
		4	499.38	0.0023
		5	567.37	0.0040
CFCF		1	101.21	0.0009
		2	125.33	0.0009
		3	248.73	0.0024
		4	258.79	0.0038
		5	290.94	0.0040
SFSF		1	99.36	0.0012
		2	120.81	0.0003
		3	251.85	0.0012
		4	257.72	0.0017
		5	289.62	0.0011
CFFF		1	29.41	0.0004
		2	49.80	0.0003
		3	156.84	0.0028
		4	182.59	0.0003
		5	191.84	0.0011

5. Conclusions

In the present study, the optimal layout of a partially treated laminated composite MR fluid sandwich plate was studied in terms of maximizing the natural frequencies and loss factors. The governing differential equations of motions were developed using finite element formulation. An optimization problem was formulated by combining finite element analysis and genetic algorithm for a partially treated sandwich plate to obtain the maximum natural frequency and loss factor corresponding to first five modes of flexural vibration with various combinations under different boundary conditions. The experimental study was conducted to validate the results in terms of natural frequencies identified at the optimization problem. A good agreement was observed among the results evaluated using the present method (FEA and GA) and measured frequencies. The optimal locations of the MR fluid pockets were identified for four different cases. In first three cases, the objective functions were formulated to seek the optimal locations of MR fluid pockets to maximize the fundamental natural frequency, fundamental loss factor and the summation of fundamental natural frequency and fundamental loss factor with equal weightage, respectively. In the Case 4, the objective function was formulated to maximize the linear combination of summation of the first five modes of natural frequencies and loss factors. The results suggest that the location of MR fluid pockets play an important role on the variation of natural frequencies and loss factors irrespective of the boundary conditions. Furthermore, CCCC end conditions yields the highest natural frequency and loss factor while CFFF end conditions yields the lowest natural frequency and loss factor, due to the flexibility of the end conditions. It was also shown that the larger distribution of the MR fluid yields the maximum natural frequency under CCCC, SSSS, CFCF and SFSF end conditions while clustering of MR fluids towards the fixed end of CFFF end conditions yields the highest loss factors. It was also demonstrated that the maximization of linear combination of fundamental natural frequency and loss factor yields almost similar pattern of MR fluids distribution as derived in the optimal layout obtained from the maximization of fundamental natural frequency. Similarly, the maximization of the linear combination of the first five modes of natural frequency and loss factors yields almost similar to the pattern of MR fluids distribution as obtained in optimal layout derived from the maximization of loss factors. This will provide the designer great flexibility in tailoring the location of MR fluid segments so as to yield the maximum natural frequency and loss factors at various modes of transverse vibration under various end conditions. Hence it was concluded that the optimization technique provides the efficient design layout of a partially treated laminated composite MR fluid sandwich plate in order to realize the efficiency of the vibration control mechanism with variable damping at critical components of large structure.

References

- Carlson, J.D. and Weiss, K.D. (1994), "A growing attraction to magnetic fluids", *Mach. Des.*, **66**(15), 61-64.
- Dogruer, U., Gordaninejad, F. and Evarensel, C.A. (2008), "A new magneto-rheological fluid damper for high-mobility multi-purpose wheeled vehicle (HMMWV)", *J. Intell. Mat. Syst. Str.*, **19**, 641-649.
- Gandhi, M.V., Thomson, B.S. and Choi, S.B. (1989), "A new generation of innovative ultra-advanced intelligent composite materials featuring electro-rheological fluids: an experimental investigation", *J. Compos. Mater.*, **23**, 1232-1255.
- Haiqing, G. and King, L.M. (1997), "Vibration characteristics of sandwich beams partially and fully treated with electrorheological fluid", *J. Intell. Mat. Syst. Str.*, **8**(5), 401-413.

- Hu, B.D., Xia, Wang. P. and Shi, Q. (2006), "Investigation on the vibration characteristics of a sandwich beam with smart composites-MRF", *World J. Modell. Simul.*, **2**, 201-206.
- Lara-Prieto, V. Parkin, R., Jackson, M., Silberschmidt, V. and Kęsy, Z. (2010), "Vibration characteristics of MR cantilever sandwich beams: experimental study", *Smart Mater. Struct.*, **19**, 015005.
- Lee, C.Y. and Jwo, K.L. (2001), "Experimental study on electrorheological material with grooved electrode surfaces", *Mater. Des.*, **22**(4), 277-283.
- Leng, J.S., Liu, S.Y., Du, S.Y., Wang, L. and Wang, D.E. (1995), "Active vibration control of smart composites featuring electro-rheological fluids", *Appl. Compos. Mater.*, **2**(1), 59-65.
- Li, Y.H., Fang, B., Li, F.M., Zhang, J.Z. and Li, S. (2011), "Dynamic analysis of sandwich plates with a constraining layer and a magnetorheological fluid Core", *Polym. Polym. Compos.*, **19**(4-5), 295-302.
- Manoharan, R., Vasudevan, R. and Jeevanantham, A.K. (2014a), "Dynamic characterization of a laminated composite magnetorheological fluid sandwich plate", *Smart Mater. Struct.*, **23**(2), 025022.
- Manoharan, R., Vasudevan, R. and Jeevanantham, A.K. (2014b), "Vibration analysis of a partially treated laminated composite magnetorheological fluid sandwich plate", *J. Vib. Control*, Online available from 14 may 2014, DOI: 10.1177/1077546314532302.
- Qiu, J. and Khajika, T. (1999), "Damping effect of multi-layer beams with embedded electrorheological fluid", *J. Intell. Mat. Syst. Str.*, **10**(7), 521-529.
- Rajamohan, V., Sedaghati, R. and Rakheja, S. (2010a), "Vibration analysis of a multi-layer beam containing magnetorheological fluid", *Smart Mater. Struct.*, **19**(1), 015013.
- Rajamohan, V., Rakheja, S. and Sedaghati, R. (2010b), "Vibration analysis of a partially treated multi-layer beam with magnetorheological fluid", *J. Sound Vib.*, **329**(17), 3451-3469.
- Rajamohan, V., Sedaghati, R. and Rakheja, S. (2010c), "Optimum design of a multilayer beam partially treated with magnetorheological fluid", *Smart Mater. Struct.*, **19**(6), 065002-15.
- Rajamohan, V., Sedaghati, R. and Rakheja, S. (2011), "Optimal vibration control of multilayer beam with total and partial MR fluid treatments", *Smart Mater. Struct.*, **20**(11), 115016.
- See, H. (2004), "Advances in electro-rheological fluids: materials, modeling and application", *J. Ind. Eng. Chem.*, **10**(7), 1132-1145.
- Sun, Q., Zhou, J.X. and Zhang, L. (2003), "An adaptive beam model and dynamic characteristics of magnetorheological materials", *J. Sound Vib.*, **261**(3), 465-481.
- Yalcintas, M. and Dai, H. (1999), "Magnetorheological and electrorheological materials in adaptive structures and their performance comparison", *Smart Mater. Struct.*, **8**, 560-573.
- Yalcintas, M. and Dai, H. (2004), "Vibration suppression capabilities of magneto-rheological materials based adaptive structures", *Smart Mater. Struct.*, **13**(1), 1-11.
- Yeh, J.Y. and Chen, L.W. (2004), "Vibration of a sandwich plate with a constrained layer and electrorheological fluid core", *Compos. Struct.*, **65**(2), 251-258.
- Yeh, J.Y. and Chen, L.W. (2007), "Finite element dynamic analysis of orthotropic sandwich plates with an electrorheological fluid core layer", *Compos. Struct.*, **78**(3), 368-376.
- Yeh, Z.F. and Shih, Y.S. (2006), "Dynamic characteristics and dynamic instability of magnetorheological based adaptive beams", *J. Compos. Mater.*, **40**(15), 1333-1359.
- Yeh, J.Y. (2013), "Vibration analysis of sandwich rectangular plates with magnetorheological elastomer damping treatment", *Smart Mater. Struct.*, **22**(3), 035010.

Appendix

The shape functions used in evaluating the stiffness and mass matrices of the sandwich plate element

$$N_{ur1} = \left[\frac{1}{4} \left(1 - \frac{x}{l} \right) \left(1 - \frac{y}{b} \right) \right]; N_{ub1} = \left[\frac{1}{4} \left(1 - \frac{x}{l} \right) \left(1 - \frac{y}{b} \right) \right]; N_{vr1} = \left[\frac{1}{4} \left(1 - \frac{x}{l} \right) \left(1 - \frac{y}{b} \right) \right];$$

$$N_{vb1} = \left[\frac{1}{4} \left(1 - \frac{x}{l} \right) \left(1 - \frac{y}{b} \right) \right]; N_{w1} = \left[\frac{1}{8} \left(1 - \frac{x}{l} \right) \left(1 - \frac{y}{b} \right) \left(2 - \frac{x}{l} - \frac{x^2}{l^2} - \frac{y}{b} - \frac{y^2}{b^2} \right) \right];$$

$$N_{\theta x1} = \left[\frac{1}{8} b \left(1 - \frac{x}{l} \right) \left(1 - \frac{y}{b} \right) \left(1 - \frac{y^2}{b^2} \right) \right]; N_{\theta y1} = \left[-\frac{1}{8} l \left(1 - \frac{x}{l} \right) \left(1 - \frac{y}{b} \right) \left(1 - \frac{x^2}{l^2} \right) \right];$$

$$N_{ur2} = \left[\frac{1}{4} \left(1 + \frac{x}{l} \right) \left(1 - \frac{y}{b} \right) \right]; N_{ub2} = \left[\frac{1}{4} \left(1 + \frac{x}{l} \right) \left(1 - \frac{y}{b} \right) \right]; N_{vr2} = \left[\frac{1}{4} \left(1 + \frac{x}{l} \right) \left(1 - \frac{y}{b} \right) \right];$$

$$N_{vb2} = \left[\frac{1}{4} \left(1 + \frac{x}{l} \right) \left(1 - \frac{y}{b} \right) \right]; N_{w2} = \left[\frac{1}{8} \left(1 + \frac{x}{l} \right) \left(1 - \frac{y}{b} \right) \left(2 + \frac{x}{l} - \frac{x^2}{l^2} - \frac{y}{b} - \frac{y^2}{b^2} \right) \right];$$

$$N_{\theta x2} = \left[\frac{1}{8} b \left(1 + \frac{x}{l} \right) \left(1 - \frac{y}{b} \right) \left(1 - \frac{y^2}{b^2} \right) \right]; N_{\theta y2} = \left[\frac{1}{8} l \left(1 + \frac{x}{l} \right) \left(1 - \frac{y}{b} \right) \left(1 - \frac{x^2}{l^2} \right) \right];$$

$$N_{ur3} = \left[\frac{1}{4} \left(1 + \frac{x}{l} \right) \left(1 + \frac{y}{b} \right) \right]; N_{ub3} = \left[\frac{1}{4} \left(1 + \frac{x}{l} \right) \left(1 + \frac{y}{b} \right) \right]; N_{vr3} = \left[\frac{1}{4} \left(1 + \frac{x}{l} \right) \left(1 + \frac{y}{b} \right) \right];$$

$$N_{vb3} = \left[\frac{1}{4} \left(1 + \frac{x}{l} \right) \left(1 + \frac{y}{b} \right) \right]; N_{w3} = \left[\frac{1}{8} \left(1 + \frac{x}{l} \right) \left(1 + \frac{y}{b} \right) \left(2 + \frac{x}{l} - \frac{x^2}{l^2} + \frac{y}{b} - \frac{y^2}{b^2} \right) \right];$$

$$N_{\theta x3} = \left[-\frac{1}{8} b \left(1 + \frac{x}{l} \right) \left(1 + \frac{y}{b} \right) \left(1 - \frac{y^2}{b^2} \right) \right]; N_{\theta y3} = \left[\frac{1}{8} l \left(1 + \frac{x}{l} \right) \left(1 + \frac{y}{b} \right) \left(1 - \frac{x^2}{l^2} \right) \right];$$

$$N_{ur4} = \left[\frac{1}{4} \left(1 - \frac{x}{l} \right) \left(1 + \frac{y}{b} \right) \right]; N_{ub4} = \left[\frac{1}{4} \left(1 - \frac{x}{l} \right) \left(1 + \frac{y}{b} \right) \right]; N_{vr4} = \left[\frac{1}{4} \left(1 - \frac{x}{l} \right) \left(1 + \frac{y}{b} \right) \right];$$

$$N_{vb4} = \left[\frac{1}{4} \left(1 - \frac{x}{l} \right) \left(1 + \frac{y}{b} \right) \right]; N_{w4} = \left[\frac{1}{8} \left(1 - \frac{x}{l} \right) \left(1 + \frac{y}{b} \right) \left(2 - \frac{x}{l} - \frac{x^2}{l^2} + \frac{y}{b} - \frac{y^2}{b^2} \right) \right];$$

$$N_{\theta x^4} = \left[-\frac{1}{8}b \left(1 - \frac{x}{l} \right) \left(1 + \frac{y}{b} \right) \left(1 - \frac{y^2}{b^2} \right) \right]; N_{\theta y^4} = \left[-\frac{1}{8}l \left(1 - \frac{x}{l} \right) \left(1 + \frac{y}{b} \right) \left(1 - \frac{x^2}{l^2} \right) \right];$$

where l and b are the length and width of the sandwich plate element.

Element stiffness matrix

$$[k^e] = \iint [B_i]^T \begin{bmatrix} A & B \\ B & D \end{bmatrix} [B_i] dx dy$$

where $[B_i]$ is the strain displacement matrix, $[A]$ is the extensional stiffness matrix which relates the resultant in-plane forces to in-plane strains, $[D]$ the bending stiffness matrix which relates the resultant bending moments to the plate curvatures, and $[B]$ is the coupling stiffness matrix which couples the force and moment terms to the mid-plane strains and mid-plane curvatures.

Element mass matrix

$$[m^e] = \iiint \rho dz [N_i]^T [N_i] dx dy, \text{ where } [N_i] \text{ is the shape function.}$$

Nomenclature

ω	Natural frequency
η	Loss factor
α	Weightage factor
pop_size	Population size
C	chromosomes
$p(c)$	Probability of the chromosomes
$cp(c)$	Cumulative probability of the chromosomes
c_1	Chromosomes selected in the selection process
c_2	Chromosomes selected for the crossover
c_3	Offspring from crossover
c_4	Offspring from mutation
p_cross	Probability of crossover
p_mut	Probability of mutation
A_{ij}	Extensional stiffness matrix
B_{ij}	Coupling stiffness matrix
D_{ij}	Bending stiffness matrix
h_t	Thickness of top layer
h_b	Thickness of bottom layer
h_c	Thickness of core layer
ρ_t	Density of top layer
ρ_b	Density of bottom layer
ρ_{cf}	Density of MR fluid core layer
ρ_{cr}	Density of rubber core layer
E_1, E_2	Young's modulus in material axes
ν_{12}, ν_{21}	Poisson's ratios in material axes
G_{12}	Shear modulus in material axes